

High-resolution optical coherence tomographic imaging using a mode-locked Ti:Al₂O₃ laser source

B. Bouma, G. J. Tearney, S. A. Boppart, and M. R. Hee

Department of Electrical Engineering and Computer Science, Research Laboratory of Electronics, Massachusetts Institute of Technology, Cambridge, Massachusetts 02139

M. E. Brezinski

Cardiac Unit, Massachusetts General Hospital and Harvard Medical School, Boston, Massachusetts 02144

J. G. Fujimoto

Department of Electrical Engineering and Computer Science, Research Laboratory of Electronics, Massachusetts Institute of Technology, Cambridge, Massachusetts 02139

Received March 30, 1995

A Kerr-lens mode-locked Ti:Al₂O₃ oscillator, optimized for minimal coherence length, is demonstrated as a high-power source for high-resolution optical coherence tomographic imaging. Dispersion compensation and heterodyne noise rejection are demonstrated to yield *in situ* images of biological tissues with 3.7- μm resolution and 93-dB dynamic range.

Many imaging modalities have been developed that permit the *in situ* visualization of biological tissues that allows one to investigate dynamic processes, facilitate the diagnosis of disease, and direct therapeutic intervention or monitor therapeutic effects. Each of these technologies has unique capabilities in terms of depth of penetration, resolution, and contrast selectivity. To date, however, few imaging techniques permit noninvasive, micrometer-scale resolution imaging at even modest depths in optically nontransparent biological tissues. Optical coherence tomography¹ (OCT) is a noninvasive cross-sectional fiber-optically based imaging technology that is currently being applied to biological tissues. OCT uses a low-coherence optical source to perform coherence-domain reflectometry of tissue microstructure. Superluminescent diode sources have been utilized extensively in ophthalmic coherence ranging and OCT systems developed for *in vivo* imaging of the anterior eye and retina^{2,3} and for coherence ranging and OCT in optically scattering tissues.⁴ Low-noise superluminescent diodes are capable of providing sub-20- μm resolution imaging at several fixed wavelengths, including 0.8 and 1.3 μm , but are limited to optical powers of a few milliwatts.⁵ Broadband fluorescence from organic dye⁶ and from Ti:Al₂O₃ (Ref. 7) have allowed 2- μm resolution ranging, but because of the inherently low brightness of these sources biological imaging has not been demonstrated. Unlike with fluorescent sources, recent developments in femtosecond mode locking of solid-state lasers permit the generation of tunable low-coherence light at single-transverse-mode power levels well in excess of 100 mW. In this Letter we demonstrate the application of a bandwidth-optimized Kerr-lens mode-locked (KLM) Ti:Al₂O₃ oscillator with < 2- μm coherence length in a high-power, high-resolution fiber-optic OCT imaging system.

Coherence-domain ranging in OCT is performed with a fiber-optic Michelson interferometer, as depicted in Fig. 1. As the length of the reference arm is scanned, interferometric modulation results at the detectors only when the phase delay of the light collected from the sample is matched, to within the source coherence length, with the phase delay incurred in the reference arm. In this way backreflection sites within the sample are localized in the longitudinal direction.⁵ If a Gaussian source line shape is assumed, the longitudinal resolution, ΔL , is given by

$$\Delta L = \frac{2 \ln(2)}{\pi} \frac{\lambda^2}{\Delta \lambda},$$

where λ is the source wavelength and $\Delta \lambda$ is the FWHM spectral width. Resolution transverse to the optical axis is given by the focal spot size within the sample, which is determined by the numerical aperture of the objective. In a manner analogous to radar, we can construct a cross-sectional image by sweeping the probe beam across the sample or by translating the sample while measuring subsequential longitudinal scans.

The suitability of a light source for OCT is determined primarily by wavelength, coherence length, brightness, and amplitude stability. Recent advances in the mode locking of solid-state lasers have resulted in the development of several attractive sources for OCT. Kerr-lens mode locking⁸ in Ti:Al₂O₃ oscillators has been shown to be capable of producing high-average-power trains of near-infrared pulses with durations < 10 fs.⁹ To date, these lasers have been exploited exclusively for the analysis of time-domain phenomena. The broad spectral range of Ti:Al₂O₃ is especially powerful for coherence-domain ranging as a source for ultrahigh spatial resolution, for intermediate resolutions and high image acquisition speeds that

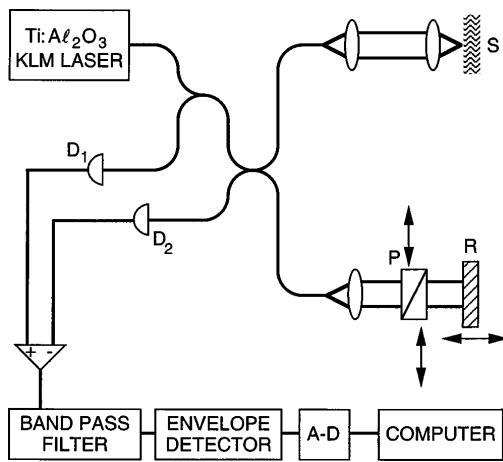


Fig. 1. Fiber-optic Michelson interferometer using a KLM Ti:Al₂O₃ laser as a short-coherence-length, high-power source. The heterodyne signal that results from the constant velocity translation of the reference mirror (R) is registered at the detectors (D₁, D₂) only when the path lengths of the sample arm (S) and the reference arm are matched to within the source coherence length. Dispersion is balanced between the two arms by a variable thickness window (P) consisting of two index-matched fused-silica prisms. A-D, analog-to-digital converter.

require high power, and for spectrally resolved tomographic imaging. In this Letter we focus on ultrahigh-resolution imaging. We have optimized the coherence length of the TiAl₂O₃ oscillator used in this experiment by minimizing phase errors resulting from the mismatch of the anomalous dispersion of the intracavity prism sequence relative to that of the corundum crystal host of the gain medium.¹⁰ Specifically, the gain crystal length is short (4 mm), and the optimum commercially available prism material (fused silica) was chosen. When the separation of the cavity focusing mirrors is adjusted so that the nonlinear cavity mode experiences less round-trip diffractive loss than the linear mode does, stable KLM operation results. As the prism configuration is adjusted to minimize residual round-trip phase error, the spectrum of the laser can be increased to fill the entire bandwidth of the dielectric resonator mirror coatings. The optimization of Kerr-lens mode locking is verified by the capability of sustaining stable mode-locked operation while the net cavity dispersion is tuned continuously from negative to positive. At an output power of 400 mW the spectrum of this laser, as shown in Fig. 2, has a width of 145 nm, corresponding to $\Delta L = 1.9 \mu\text{m}$.

Because the signal measured by OCT is the cross correlation of the electric fields returned from the interferometer arms, dispersion incurred before both arms does not affect the resolution. In contrast to time-domain applications, this permits the laser to be fiber-optically delivered to the interferometer. Dispersion imbalance between the interferometer arms, however, must be precisely canceled in order to preserve resolution.⁷ An imbalance equivalent to an additional 0.5 mm of fused silica in one interferometer arm results in a broadening in the cross-correlation width of approximately 17%. To allow dispersion balancing, we insert a fused-silica prism pair with faces contacted

and index matched to form a variable-thickness window in the reference arm (Fig. 1). The width of the cross-correlation function is minimized by translating the prisms along their contacted faces. This simple adjustment compensates for differences in fiber length, collimating lens, and microscope objectives between the interferometer arms.

The transmission bandwidth of the optical and electronic systems is also critical to preserving the longitudinal resolution of the OCT device. The optical fibers and splitters of the current system are industry standard devices and are not matched to the Ti:Al₂O₃ laser source bandwidth. The narrowed optical spectrum measured at the detectors is shown by the dotted curve in Fig. 2. The bandpass filter and envelope detector (Fig. 1) have been designed to support a 10-kHz bandwidth centered at the 50-kHz Doppler frequency, which results from a reference mirror velocity of 20 mm/s. We measured the longitudinal system response in air to be 3.7 μm FWHM by placing a single surface reflector in the sample arm. The measured resolution corresponds to the resolution predicted from the Fourier transform of the power spectrum measured at the detector and verifies the accuracy of the dispersion balance between the interferometer arms.

The high amplitude noise of the Ti:Al₂O₃ oscillator relative to that of superluminescent diode sources necessitates the use of dual-detector heterodyne detection to produce a shot-noise-limited signal-to-noise ratio (SNR). At the 50-kHz interferometric modulation frequency of the current OCT system, the Ti:Al₂O₃ oscillator amplitude noise is measured to be 37 dB above the shot-noise level. Dual balanced detection¹¹ allows this noise to be canceled to within 4 dB of shot noise. In the shot-noise limit the SNR of the system¹² is determined by the number of photons scattered from the sample that reach the detectors in a time interval determined by the inverse of the detection bandwidth:

$$\text{SNR} = 10 \ln \left(\frac{\eta P_{\text{SAM}}}{\hbar \omega \text{NEB}} \right),$$

where η is the detector efficiency, $\hbar \omega$ is the energy per photon, P_{SAM} is the power of the light scattered

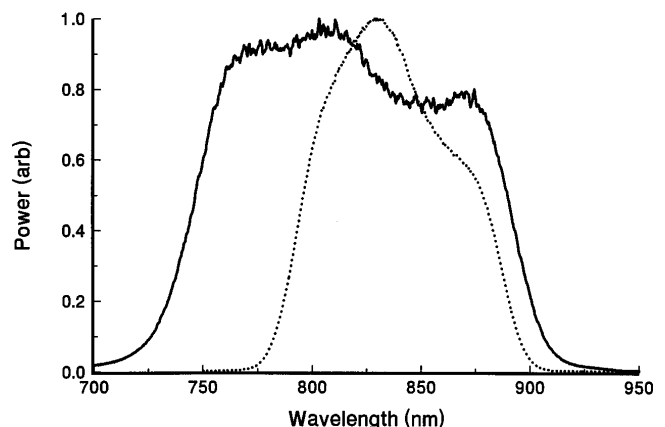


Fig. 2. Spectra of the output of the Ti:Al₂O₃ oscillator (solid curve) and of the field transmitted to the detector ports of the interferometer (dotted curve).

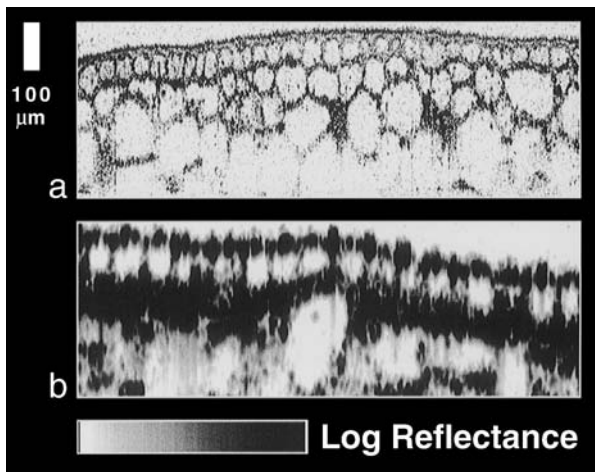


Fig. 3. Tomographic images of onion produced by a, the high-resolution Ti:Al₂O₃ OCT system and b, a superluminescent diode OCT system. The numerical apertures of the objectives for these two systems were not equivalent but were chosen so that transverse resolution was matched to the axial resolution. The uppermost layer of cells has an average diameter of 40 μm and a cell wall thickness of $\sim 5 \mu\text{m}$.

from the sample to the detector, and NEB is the noise-equivalent bandwidth. The bandwidth of the detection electronics, $\Delta\nu$, must be specified commensurate with the source optical bandwidth, indicating that for fixed SNR higher optical power is required for higher-resolution optical sources. Losses that are due to backreflections from fiber connectors and improperly coated collimating objectives in the current system limit the obtained SNR to 93 dB, less than the predicted 110-dB value with 1 mW of optical power delivered to the sample but sufficient to provide high-quality images of most biological samples. A redesign of the optical fiber system is currently being investigated to overcome these limitations.

OCT images of an onion performed with the standard-resolution superluminescent diode source system of Ref. 8 (Fig. 3b) and with the KLM Ti:Al₂O₃ system (Fig. 3a) demonstrate the comparative resolutions of these systems. In both images the transverse resolution determined by the objectives is approximately matched to the longitudinal resolution as determined by the system bandwidth. In Fig. 3a the optical beam diameter is 5 μm in the focal plane that is centered on the first horizontal cell layer. The corresponding confocal parameter is 40 μm , the approximate dimension of the cells in this layer. At greater depths, resolution degradation as a result of divergence becomes apparent. Translating the focal plane permits high-resolution imaging to a depth of $\sim 600 \mu\text{m}$ in onion, where multiple scattering becomes significant. The confocal parameter in Fig. 3b is 350 μm . Both of these images were acquired in 2.5 s by sampling 120 vertical and 360 horizontal pixels. No image processing or averaging was performed.

In conclusion, a bandwidth-optimized KLM Ti:Al₂O₃ oscillator coupled to a fiber-optic OCT system that permits high-resolution, high-dynamic-range, non-

contact imaging of biological structures has been demonstrated. Recent advances in the development of compact and diode-pumped solid-state sources should allow the extension of this work to a clinically viable imaging system. Additionally, the application of Kerr-lens mode locking to other solid-state laser materials will provide high-power, short-coherence-length sources at other biologically significant wavelengths such as 1.3 μm from Cr:forsterite and 1.5 μm from Cr:YAG.

The authors acknowledge scientific discussions with E. Swanson and J. Izatt. This research is supported in part by National Institutes of Health grant NIH-5-R01-GM35459-09 and U.S. Office of Naval Research Medical Free Electron Laser Program grant N00014-94-1-0717.

References

1. D. Huang, E. A. Swanson, C. P. Lin, J. S. Schuman, W. G. Stinson, W. Chang, M. R. Hee, T. Flotte, K. Gregory, C. A. Puliafito, and J. G. Fujimoto, *Science* **254**, 1178 (1991).
2. E. A. Swanson, J. A. Izatt, M. R. Hee, D. Huang, C. P. Lin, J. S. Schuman, C. A. Puliafito, and J. G. Fujimoto, *Opt. Lett.* **18**, 1864 (1993); J. A. Izatt, M. R. Hee, E. A. Swanson, C. P. Lin, D. Huang, J. S. Schuman, C. A. Puliafito, and J. G. Fujimoto, *Arch. Ophthalmol.* **112**, 1584 (1994).
3. C. K. Hitzenberger, *Invest. Ophthalmol. Vis. Sci.* **32**, 616 (1991); A. F. Fercher, K. Mengedocht, and W. Werner, *Opt. Lett.* **13**, 186 (1988).
4. G. J. Tearney, M. E. Brezinski, M. R. Hee, B. Bouma, J. A. Izatt, J. F. Southern, E. A. Swanson, and J. G. Fujimoto, in *Conference on Lasers and Electro-Optics*, Vol. 15 of 1995 OSA Technical Digest Series (Optical Society of America, Washington, D.C., 1995), paper CThN3.
5. K. Takada, I. Yokohama, K. Chida, and J. Noda, *Appl. Opt.* **26**, 1603 (1987); R. C. Youngquist, S. Carr, and D. E. N. Davies, *Opt. Lett.* **12**, 158 (1987).
6. H.-H. Liu, P.-H. Cheng, and J. Wang, *Opt. Lett.* **18**, 678 (1993).
7. X. Clivaz, F. Marquis-Weible, and R.-P. Salathé, *Proc. Soc. Photo-Opt. Instrum. Eng.* **2083**, 19 (1994).
8. D. E. Spence, P. N. Kean, and W. Sibbett, *Opt. Lett.* **16**, 42 (1991); L. Spinelli, B. Couillaud, N. Goldblatt, and D. K. Negus, in *Conference on Lasers and Electro-Optics*, Vol. 10 of 1991 OSA Technical Digest Series (Optical Society of America, Washington, D.C., 1991), paper CPDP7.
9. J. Z. Zhou, G. Taft, C. P. Huang, M. M. Murnane, and H. C. Kapteyn, *Opt. Lett.* **19**, 1149 (1994); J. D. Harvey, J. M. Dudley, P. F. Curley, C. Spielmann, and F. Krausz, *Opt. Lett.* **19**, 972 (1994).
10. B. E. Bouma, Ph.D. dissertation (University of Illinois, Chicago, Ill., 1993); M. T. Asaki, C. P. Huang, D. Garvey, J. Zhou, H. C. Kapteyn, and M. M. Murnane, *Opt. Lett.* **18**, 977 (1993).
11. G. L. Abbas, V. W. S. Chan, and T. K. Yee, *Opt. Lett.* **8**, 419 (1983); P. Beaud, J. Schütz, W. Hodel, H. P. Weber, H. H. Gilgen, and R. P. Salathé, *IEEE J. Quantum Electron.* **25**, 755 (1989).
12. E. A. Swanson, D. Huang, M. R. Hee, J. G. Fujimoto, C. P. Lin, and C. A. Puliafito, *Opt. Lett.* **17**, 151 (1992).